Mon. Not. R. Astron. Soc. 000, 1–15 (2010) Printed 8 April 2011 (MN LATEX style file v2.2)

Measuring Redshift-Space Distortions using Photometric Surveys

Ashley J. Ross⋆[1], Will J. Percival[1], Martín Crocce[2], Anna Cabré[3], & Enrique Gaztañaga[2]
[1]*Institute of Cosmology & Gravitation, Dennis Sciama Building, University of Portsmouth, Portsmouth, PO1 3FX, UK*
[2]*Institut de Ciències de l'Espai, CSIC/IEEC, F. de Ciències, Torre C5 par-2, Barcelona 08193, Spain*
[3]*Center for Particle Cosmology, University of Pennsylvania, 209, South 33rd Street, Philadelphia, PA, 19104, USA*

Accepted by MNRAS

ABSTRACT
We outline how redshift-space distortions (RSD) can be measured from the angular correlation function $w(\theta)$, of galaxies selected from photometric surveys. The natural degeneracy between RSD and galaxy bias can be minimized by comparing results from bins with top-hat galaxy selection in redshift, and bins based on the radial position of galaxy pair centres. This comparison can also be used to test the accuracy of the photometric redshifts. The presence of RSD will be clearly detectable with the next generation of photometric redshift surveys. We show that the Dark Energy Survey (DES) will be able to measure $f(z)\sigma_8(z)$ to a 1σ accuracy of $(17 \times b)\%$, using galaxies drawn from a single narrow redshift slice centered at $z = 1$. Here b is the linear bias, and f is the logarithmic rate of change of the linear growth rate with respect to the scale factor. Extending to measurements of $w(\theta)$ for a series of bins of width $0.02(1 + z)$ over $0.5 < z < 1.4$ will measure γ to a 1σ accuracy of 25%, given the model $f = \Omega_m(z)^\gamma$, and assuming a linear bias model that evolves such that $b = 0.5 + z$ (and fixing other cosmological parameters). The accuracy of our analytic predictions is confirmed using mock catalogs drawn from simulations conducted by the MICE collaboration.

Key words: Cosmology – Observational: methods, large-scale structure

1 INTRODUCTION

The statistical analysis of redshift-space distortions (RSD) provides constraints on the build-up of cosmological structure (see Hamilton 1998 for a review). RSD are apparent anisotropic patterns of galaxies formed when redshifts are converted into galaxy distances assuming the Hubble flow: coherent comoving peculiar velocities are translated into apparent distributions of galaxies. On small distance scales ($\sim 1\,h^{-1}\,\mathrm{Mpc}$), we see the well-known "finger of god" effect (see, e.g., Jackson 1972), due to orbital velocities of galaxies that are members of bound structures. On larger distance scales, galaxies move with structure growth, leading to an apparent excess in the clustering strength along the line-of-sight.

Following linear theory, the large-scale effect of RSD on 2-point statistics can be modelled as a simple enhancement of the galaxy overdensity field (Kaiser 1987). This leads to an anisotropic correlation function (Hamilton 1992) that is a function of both radial and transverse separations. The excess line-of-sight clustering strength depends on the amplitude of the matter velocity field that, following linear theory, is usually parametrised by $f(z)\sigma_{8,\mathrm{mass}}(z)$, where f is the rate of change of the linear growth rate $f \equiv d\log G/d\log a$, G is the linear growth rate, a is the scale factor of the Universe, and $\sigma_{8,\mathrm{mass}}(z)$ is the root mean square amplitude of fluctuations in the matter overdensity field in spheres of radius $8\,h^{-1}\,\mathrm{Mpc}$. We will now drop the "mass" label as we will only refer to $\sigma_8(z)$ as normalising the matter fluctuation field from here-on. Without the RSD, the amplitude of the real-space galaxy overdensity field can be parametrised by $b(z)\sigma_8(z)$, where $b(z)$ is the bias of the galaxies. For ΛCDM cosmologies, to a good approximation, $f(z) \equiv \Omega_m(z)^\gamma$ (Linder 2005) with $\gamma = 0.557$, and measurements of $\xi^s(\mathbf{r})$ can be used to test the standard cosmological model — either by translating them into measurements of $f(z)$ using an external constraint on the galaxy bias or performing a dual fit for $b(z)\sigma_8(z)$ and $f(z)\sigma_8(z)$ (while accounting for the implied change in $\sigma_8(z)$ when $f(z)$ is changed).

RSD measurements have traditionally been confined to spectroscopic redshift surveys, where accurate redshifts have been obtained for a sample of galaxies: measurements from the 2dF Galaxy Redshift Survey (2dFGRS; Colless et al. 2003) and the Sloan Digital Sky Survey (SDSS; York et al. 2000) are given by Peacock et al. (2001); Hawkins et al. (2003); Percival et al. (2004); Pope et al. (2004); Zehavi et al. (2005); Okumura et al. (2008); Cabre & Gaztanaga (2009) for example, and RSD have recently been detected at higher redshift (Guzzo et al. 2009; Blake et al. 2010).

Photometric surveys are usually overlooked when it comes to RSD measurements because the photometric redshift errors are thought to wash out any RSD signal. Without question, these errors will significantly degrade the imprint of RSD. However, it is timely to investigate the extent to which this is true given both the high-quality of upcoming data from the

⋆ Email: Ashley.Ross@port.ac.uk

Dark Energy Survey (DES www.darkenergysurvey.org), the Panoramic Survey Telescope and Rapid Response System (PanStarrs pan-starrs.ifa.hawaii.edu), and the Large Synoptic Survey Telescope (LSST www.lsst.org), and recent theoretical analyses that have investigated the effects of RSD on projected clustering measurements.

If galaxy redshifts are used to select samples, then we see redshift-space effects in angular/projected clustering measurements, even though the angular positions of galaxies are unchanged (Fisher et al. 1993; Nock et al. 2010, hereafter N10). Corrections for these effects were recently applied to angular power-spectra analyses of the SDSS by Blake et al. (2007), Padmanabhan et al. (2007), and Thomas et al. (2010); the latter of whom have used the corrections to place constraints on f.

Working in configuration space, these corrections have been shown to agree with $w(\theta)$ and its covariance calculated with mock photometric redshift catalogs (N10, Crocce et al. 2010b, hereafter C10). This effect arises because RSD impart coherent fluctuations in galaxy density along any redshift-dependent boundary imposed on the galaxies. Correct treatment of the redshift-space distortions is extremely important, as studies suggest that the most precise (non-RSD) cosmological constraints are obtained from using narrow redshift bins (Sanchez et al. 2010), which also give the strongest RSD signal (N10, C10).

N10 have shown that constructing galaxy samples using *pair-centre* binning removes the effects of RSD. Such a binning scheme does not consider the individual redshift of a galaxy, but rather the average redshift of (or distance to) the pair of galaxies. Thus, a pair-centre binning scheme with $0.45 < z < 0.55$ will include all of the galaxy pairs with average redshifts between 0.45 and 0.55. In standard 'top-hat' binning, all of the galaxies with redshifts between 0.45 and 0.55 would be included. The symmetry imparted by the pair centre binning is sufficient to remove the effect of RSD.

RSD and distortions caused by using the wrong geometrical model when analysing data in three dimensions (the Alcock-Palczynski (AP) effect Alcock & Paczynski 1979) give rise to similar distortions in the measured clustering (Ballinger et al. 1996; Simpson & Peacock 2009), although the strength of the degeneracy depends on the cosmological assumptions used in the data analysis (Samushia et al. 2011). Thus, in general, analyses of RSD using 3D data either have to be performed simultaneously with geometrical measurements, or utilise (and rely on) more precise geometrical constraints. The measured angular correlation function, which only depends on redshifts and angles, does not depend on the cosmological model to be fitted. Fitting models to the measured angular clustering is therefore considerably simpler.

In this work we investigate the precision to which one can measure cosmological structure growth using galaxy samples with photometric redshifts. In Section 2, we present the theoretical modelling we employ to estimate angular correlation functions of galaxies, $w(\theta)$ and their error, for different galaxy binning schemes. In Section 3, we test our analytic error predictions against mock catalogs produced by the MICE simulation and show the importance of including non-linear effects when measuring $f(z)\sigma_8(z)$. In Section 4, we determine the precision to which $f(z)\sigma_8(z)$ can be measured for a survey similar to DES using redshift bins of different sizes and mean redshifts and galaxies with various mean photometric redshift errors and linear bias. In Section 5, we test the robustness of the measurements against changes in the cosmology and systematics in the photometric redshifts and we show how comparing measurements using standard binning schemes and those using pair-centre binning measurements can test the accuracy of the photometric redshifts. We conclude in Section 6. Where appropriate we assume a flat ΛCDM model with $\Omega_m = 0.25$, $h = 0.7$, and $\Omega_b = 0.045$.

2 MODELING ANGULAR CORRELATION FUNCTIONS

For a sample of galaxy pairs, the angular-correlation function $w(\theta)$, can be modeled by integrating the redshift-space correlation-function $\xi^s(\mathbf{r})$, over the joint distribution of galaxy pairs $f(z_1, z_2)$, (Phillipps et al. 1978):

$$w(\theta) = \int dz_1 \int dz_2 f(z_1, z_2) \xi^s \left[\mathbf{r}(\theta, z_1, z_2)\right], \quad (1)$$

where the galaxy separation $\mathbf{r}$ is a function of the angular separation of the galaxies θ and their redshifts z_1 and z_2. For a binning scheme based on galaxy position (such as top-hat binning), we can separate the selection function for the two galaxies. We can then replace $f(z_1, z_2)$ by $n(z_1)n(z_2)$, where $n(z)$ is the normalized true redshift distribution, in the above expression. We note that, in practice, $n(z)$ is an estimate usually obtained from the photometric redshifts and their errors. We investigate potential systematics due to this estimation in Section 5.1.

For the pair-centre binning, $f(z_1, z_2)$ can be replaced by $n_{pc}(z_1)n_d(|z_1 - z_2|)$, where $n_{pc}(z)$ is the normalized distribution of pair centres and $n_d(\Delta z)$ is the normalized distribution of pair separations (in redshift; note that the tophat $w(\theta)$ is recovered when integrating over $n_{pc}(z_1)n_d(|z_1 - z_2|)$ when z_1 and z_2 are restricted to lie within the tophat bounds). We incorporate the photometric redshifts into $f(z_1, z_2)$, working with a redshift-space correlation function, rather than photometric redshift-space one, so the functions $n(z)$ and $f(z_1, z_2)$ depend on the photometric redshift error. For simplicity these errors are assumed to be Gaussian with standard deviation σ_z. In practice, this means that we Monte Carlo sample the true redshift distribution twice, and then Monte Carlo sample the respective Gaussians to find two positions in photometric redshift space. If the pair-centre of these positions lies within the photometric redshift bin, the true redshift pair-centre and true redshift separation is added to its respective distribution (and the respective distributions are then normalized). See N10 for further details.

In this work, we only consider the plane-parallel approximation to the geometry, and assume that $\xi^s(r)$ is given by (Hamilton 1992)

$$\xi^s(\mu, r) = \xi_o(r)P_o(\mu) + \xi_2(r)P_2(\mu) + \xi_4(r)P_4(\mu), \quad (2)$$

where

$$\xi_o(r) = (b^2 + \frac{2}{3}bf + \frac{1}{5}f^2)\xi(r), \quad (3)$$

$$\xi_2(r) = (\frac{4}{3}bf + \frac{4}{7}f^2)[\xi(r) - \xi'(r)], \quad (4)$$

$$\xi_4(r) = \frac{8}{35}f^2[\xi(r) + \frac{5}{2}\xi'(r) - \frac{7}{2}\xi''(r)], \quad (5)$$

P_ℓ are the standard Legendre polynomials, and

$$\xi' \equiv 3r^{-3}\int_0^r \xi(r')(r')^2 dr' \quad (6)$$

$$\xi'' \equiv 5r^{-5}\int_0^r \xi(r')(r')^4 dr', \quad (7)$$

b is the large-scale bias of the galaxy population being considered and $\xi(r)$ is the isotropic 3-dimensional, real-space correlation function. The factor μ is the cosine of the angle between the separation

along the line of sight and the transverse separation. We calculate $\xi(r)$ by Fourier transform from a power spectrum calculated as described in Eisenstein & Hu (1998) and include the non-linear modelling given in equation 10 of C10.

The model we employ makes some strong assumptions (linear RSD, linear bias, weak non-linear gravity). We note that its application to projected/angular correlation functions is well tested with simulation (N10, C10) and has been shown to be a good fit to measured $w(\theta)$ (see, e.g., Ross et al. 2007, 2008, 2010b for discussions of the range of scales over which measurements of angular clustering are well-fit by a linear bias model and, e.g., Samushia et al. 2011 for a discussion of the limits to which the linear RSD model is valid).

Each moment of $\xi(r)$ entering Eq. 2 is normalised to the standard correlation function, and hence its amplitude is fixed by $\sigma_8^2(z)$. Any measurements of $b(z)$ or $f(z)$ calculated using this model are therefore perfectly degenerate with the value of $\sigma_8(z)$. It is therefore most convenient for our purposes to parametrize this model with two, separate, factors: $b(z)\sigma_8(z)$ and $f(z)\sigma_8(z)$ (e.g. Song & Percival 2009).

Eq. 1 shows that binning schemes act as "moments" of the anisotropic redshift-space correlation function: each provides an integral of this function weighted by a different distribution of angles to the line-of-sight. The binning schemes therefore work in a similar way to the Legendre polynomials in the standard definition of the anisotropic correlation function. Comparing results from different schemes such as considering measurements from both the top-hat and pair-centre schemes, would allow the simultaneous measurement of both $b(z)\sigma_8(z)$ and $f(z)\sigma_8(z)$ (when accounting for the covariance between these measurements).

2.1 Errors and Covariance

Recent work has considered the problem of analytically calculating covariances for angular/projected clustering measurements (Cohn 2009, C10). In order to set constraints on how well future surveys will measure the angular clustering, we follow the approach of C10, which is based on the angular power spectrum for redshift slice i, which we denote $C_{\ell,i}$.

The error on the full-sky angular power spectrum, C_ℓ, is given by (see, e.g., Dodelson 2003)

$$\sigma^2(C_\ell) \equiv \langle C_\ell^2\rangle - \langle C_\ell\rangle\langle C_\ell\rangle \quad (8)$$

$$= \frac{2}{(2\ell+1)}\left(C_\ell + 1/\bar{n}\right)^2 \quad (9)$$

where $\bar{n}$ is number density of objects per steradian. The predicted variance of the cross-power spectrum, $C_\ell^{i,j}$, between samples i and j is given by (see, e.g., eqs. 18 and 19 of White et al. 2009)

$$\sigma^2(C_\ell^{i,j}) = \frac{1}{(2\ell+1)} \times \left[(C_\ell^{i,j})^2 + (C_\ell^i + 1/\bar{n}_i)(C_\ell^j + 1/\bar{n}_j)\right]. \quad (10)$$

Thus, given that

$$w_{i,j}(\theta) = \sum_{\ell\geqslant 0}\left(\frac{2\ell+1}{4\pi}\right)P_\ell(cos\theta)C_\ell^{i,j}, \quad (11)$$

and that the effect of only observing a fraction of the sky, f_{sky}, is well approximated by simply dividing $\sigma^2(C_\ell)$ by f_{sky} (see, e.g., C10), the covariance (that we denote Cov) between measurements of the angular cross-correlation function at θ and θ' between redshift slices i and j (that is the auto-correlation in the case $i = j$) can be modelled as

$$\mathrm{Cov}_{i,j,\theta,\theta'} \equiv \langle w_{i,j}(\theta)w_{i,j}(\theta')\rangle - \langle w_{i,j}(\theta)\rangle\langle w_{i,j}(\theta')\rangle \quad (12)$$

$$= \sum_{\ell\geqslant 0}\frac{(2\ell+1)^2}{f_{sky}(4\pi)^2}P_\ell(\cos\theta)P_\ell(\cos\theta')\sigma^2(C_\ell^{i,j}) + \frac{\delta_{\theta,\theta'}}{n_p} \quad (13)$$

where n_p is the number of galaxy pairs (that can be determined from the number density and angular size of the bin) and $\delta_{\theta,\theta'}$ is the Kronecker delta.

Given $P(k)$, the $C_{\ell,i,j}$ spectra can be calculated via (see, e.g., Fisher et al. 1993; Padmanabhan et al. 2007)

$$C_\ell^{i,j} = \frac{2}{\pi}\int k^2 dk P(k)\Psi_{\ell,i}(k)\Psi_{\ell,j}(k), \quad (14)$$

where $\Psi_{\ell,i}$ is given by

$$\Psi_{\ell,i}(k) = \Psi^r_{\ell,i} + \int dz n_i(z)D(z)j_\ell(k\chi(z)), \quad (15)$$

and j_ℓ is the spherical Bessel function of order ℓ and

$$\Psi^r_{\ell,i}(k) = f/b\int dz\, n_i(z)D(z)\left[\frac{(2\ell^2+2\ell-1)}{(2\ell+3)(2\ell-1)}j_\ell(k\chi(z)) - \frac{\ell(\ell-1)}{(2\ell-1)(2\ell+1)}j_{\ell-2}(k\chi(z)) - \frac{(\ell+1)(\ell+2)}{(2\ell+1)(2\ell+3)}j_{\ell+2}(k\chi(z))\right]. \quad (16)$$

This set of equations provides the full covariance matrix in both scale and redshift, as required in order to make measurements of $f(z)\sigma_8(z)$ at multiple redshifts.

2.2 Pair-Centre Covariance

For the pair-centre binning, determining the covariance is not as straightforward. We can produce an approximate solution by calculating the variances of all of the thin slices in photometric redshift that would contribute to the pair-centre measurement and all of the co-variances between these slices. Given a photometric redshift survey, one can split it into very narrow consecutive shells of width δs in photometric redshift located at

$$s_i = \delta s \times i \quad (i = 0, \infty). \quad (17)$$

If one wishes to estimate the pair-centre angular correlation function, w_{pc}, in a bin centered at s_b of width Δs_b (in photometric redshift space), the condition for a pair of galaxies lying in bins i and j to enter the selection is

$$y_{ij} = |\bar{s}_{ij} - s_b|/\Delta s_b \leqslant 1 \quad (18)$$

with $\bar{s}_{ij} = \delta s \times (i+j)/2$ the mean photo-z of the galaxy pair. Thus the condition can be implemented by a $\Theta(y)$ function giving 1 if $y \leqslant 1$ and 0 otherwise.

The pair-centre correlation can be estimated as,

$$w_{pc}(\theta) = \frac{\sum_i\sum_{j\geqslant i} n(z_i)n(z_j)w_{i,j}(\theta)\Theta(y_{ij})}{\sum_i\sum_{j\geqslant i} n(z_i)n(z_j)\Theta(y_{ij})} \quad (19)$$

where $w_{i,j}(\theta)$ is the angular cross-correlation function between bins i, j and $n(z_i)$ is the value of the overall redshift distribution $n(z)$ (i.e., the redshift distribution of sources over the entire survey being considered) at redshift z_i with $C_\ell^{i,j}$ calculated as described by Eqs. 14-16, with $n_i(z)$ in Eq. 15 being the true redshift distribution of the thin slice in photometric redshift space, and the covariance of $w_{i,j}(\theta)$, $\mathrm{Cov}_{i,j}(\theta,\theta')$, is therefore given by Eq. 13. Thus, one can calculate all of the $\mathrm{Cov}_{i,j}(\theta,\theta')$ contributing to the sum in Eq. 19. In order to determine $\mathrm{Cov}_{pc}(\theta,\theta')$, one must account for the covariance between $w_{h,i}(\theta)$ and $w_{j,k}(\theta)$, which we

denote $\mathrm{Cov}_{h,i,j,k}$. We can estimate $\mathrm{Cov}_{h,i,j,k}$ by calculating the "overlap", $O_{h,i,j,k}$, of the four thin photometric redshift shells,

$$O_{h,i,j,k} = \frac{\int dz n_h(z) n_i(z) n_j(z) n_k(z)}{\int dz n_h^2(z) n_i^2(z)}, \quad (20)$$

and assuming

$$\mathrm{Cov}_{h,i,j,k} = O_{h,i,j,k} \mathrm{Cov}_{h,i}(\bar{n} = \infty) \quad (21)$$

where we set $\bar{n} = \infty$ since the covariance between the separate C_ℓ measurements should not have a shot-noise contribution. We thus estimate

$$\mathrm{Cov}_{pc} = \frac{1}{W_t} \sum_{i,j \geqslant i} n^2(z_i) n^2(z_j) \mathrm{Cov_{i,j}} \Theta(y_{ij}) + \frac{1}{W_t} \sum_{h,i \geqslant h,j,k > i} n(z_h) n(z_i) n(z_j) n(z_k) \mathrm{Cov_{h,i,j,k}} \Theta(y_{hi}) \Theta(y_{jk}) \quad (22)$$

where we use $\sum_{i,j}$ as shorthand for $\sum_i \sum_j$ and

$$W_t = \sum_{h,i \geqslant h,j,k > i} n(z_h) n(z_i) n(z_j) n(z_k) \Theta(y_{hi}) \Theta(y_{jk}). \quad (23)$$

This approximation is validated by comparisons with mock catalogs in section 3.

We estimate the covariance between the top hat and pair-centre binning by assuming the correlation, $\mathrm{Cov}_{pc,TH} / \sqrt{\mathrm{Cov}_{pc} \mathrm{Cov}_{TH}}$, between the measurements is equal to the ratio of the effective volume (given by Eq. 5 of Tegmark 1997) of the galaxies used in each binning scheme. We find this correlation varies between $1/7$ and $1/2$, depending on the specific bin widths and median redshift. We find that these values are consistent with the covariance we find in the mocks used in Section 3.1, though the mocks do exhibit some scale dependence. Allowing the covariance to change by as much 25% does not affect any of the conclusions of this work, but this issue is worthy of further study in the future.

2.3 Estimating Errors for DES

As a specific example, we now consider the sensitivity of the angular correlation functions expected to be measured for DES. As in N10, we take the overall selection of DES galaxies to have the form

$$n_{DES}(z) \propto (\frac{z}{0.5})^2 exp(-\frac{z}{0.5})^{1.5}, \quad (24)$$

and assume that DES will observe 300 million galaxies over 1/8th of the sky[1]. These galaxies are assumed to be unbiased on average, that is $b = 1$. We will consider the dependence of our conclusions on bias in Section 4.1.

Because the DES galaxy density is high, the predicted error for clustering measurements at a given equivalent physical scale (i.e, $\sim \chi(z)\theta$, where $\chi(z)$ is the comoving distance to redshift z), for bins that are of the same order as σ_z, will be driven almost entirely by the median redshift of the sample: the shot noise term in Eq. 13 has a negligible impact on the final error. Thus, for DES, $\mathrm{Cov}_{\theta,\theta'} \propto C_\ell^2$, and we would expect the same percentage error regardless of the width of the redshift bin for both top-hat and pair-centre binning. Note that this argument will break down around the BAO scale where the angular correlation crosses from positive to negative and consequently the proportionality arguments do not hold. Also, moving to smaller bins will not necessarily provide significant additional signal because results will be correlated through the photometric redshift errors.

We assume Gaussian photometric redshift errors, σ_z, of $0.03(1+z)$. Although the average σ_z of the full sample of DES galaxies at these redshifts is predicted to be closer to $0.05(1+z)$ than $0.03(1+z)$ (see Banerji et al. 2008, Fig. 1 of C10), a slight reduction in the number of galaxies used can have a large effect on the mean value of σ_z. As discussed above, the density of galaxies is high so results are cosmic variance and photometric redshift limited: we can therefore reduce the sample density without a significant increase in noise. But the ability to measure RSD does depend strongly on the width of the redshift distribution: Consequently, galaxy samples should be constructed to have minimal average σ_z (by selecting, for example, primarily early-type galaxies). The ease of redshift determination for these galaxies can lead to significant gains: SDSS galaxies with $0.2 < z < 0.3$ and $M_r < -21.2$ have an average σ_z of 0.041, but if one removes all of the galaxies with σ_z greater than $0.053(1+z)$, this is reduced to 0.03 and 82% of the galaxies are left in the sample. (This sample was studied by Ross et al. 2010a, and the estimated photometric redshift errors were consistent with the measured clustering.)

Fig. 1 compares model correlation functions (multiplied by θ^2 for clarity), calculated by directly projecting the 3D correlation function. These were calculated for galaxies within a photometric redshift bin $0.45 < z < 0.55$ and $\sigma_z = 0.03(1+z)$. We plot models for a top-hat bin in real-space (red) and redshift-space (black), and for pair-centre binning (blue). We also display the theoretical uncertainties, as predicted via Eq. 13 for the top-hat bin and Eq. 22 for the pair-centre bin. The signal-to-noise is considerably worse for the pair-centre binning.

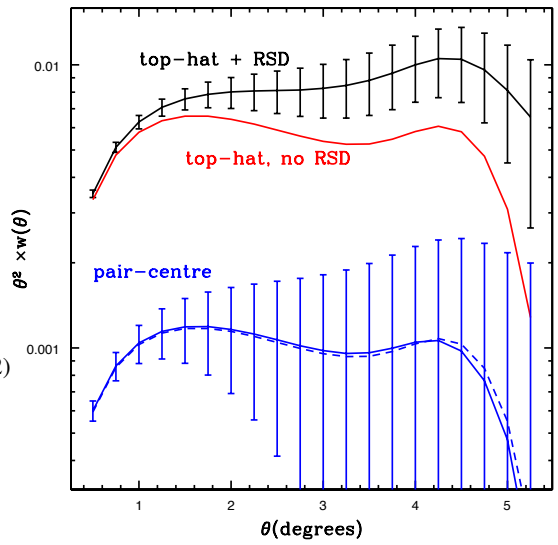

Figure 1. Model angular correlations functions (multiplied by θ^2 for clarity), calculated directly using Eq. (1) from the 3D correlation function. These are for distributions of galaxies within the photometric redshift bin $0.45 < z < 0.55$ and assume $\sigma_z = 0.03(1+z)$. The black line is for a top-hat bin when redshift-distortions (RSD) are included, its and theoretical uncertainties are also displayed (calculated via Eq. 13) , while the red line was calculated without RSD. The solid blue line is for a pair-centre binning, with its theoretical uncertainties (calculated via Eq. 22) also displayed. The dashed-blue line displays the top-hat, no RSD prediction divided by 5.62.

[1] We thank the DES LSS working group for providing these estimations.

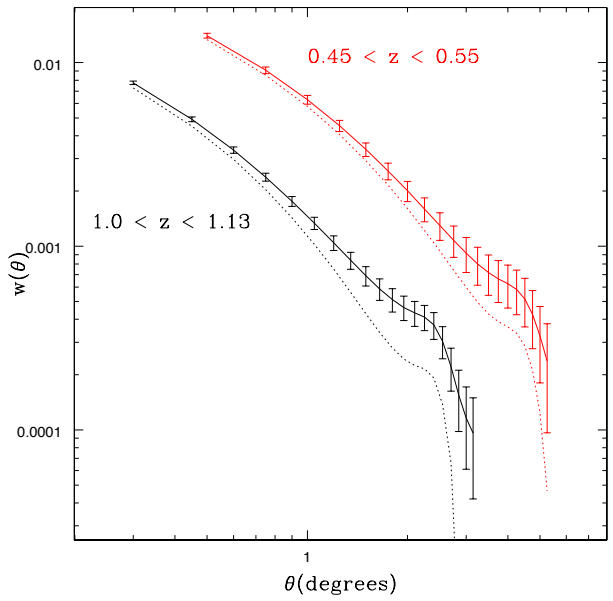

Figure 2. Model angular correlation functions for galaxies drawn from the DES in top-hat bins with photometric redshifts $1.0 < z_{\rm phot} < 1.13$ (black) and $0.45 < z_{\rm phot} < 0.55$ (red). The solid curves include RSD, dashed lines do not. Error bars, which are only plotted for models with RSD, were calculated using Eq. (13).

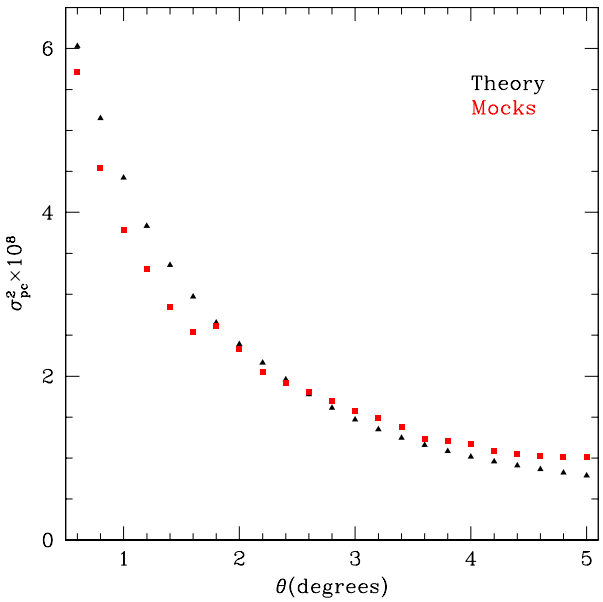

Figure 3. The variance (σ^2) of the angular correlation function in the pair-centre bin $0.475 < z_{pc} < 0.525$ for objects with a DES-like distribution, determined from 125 mock realizations (black triangles) and estimated theoretically (using Eq. 22) .

The dashed line in Fig. 1 represents the case where we divide the real-space top-hat prediction by 5.62. This illustrates that the shape of the pair-centre measurement is nearly identical to that of the top-hat without redshift space distortions. We find this to be true in general when the width of the pair-centre bin matches the width of the top-hat bin. While we find we can apply slightly more narrow redshift bounds to the pair-centre bin and obtain models that are slightly better matched, for simplicity, we will always apply the same redshift bounds when comparing model pair-centre and top-hat $w(\theta)$.

Fig. 2 presents the predicted angular correlation functions for DES, with and without RSD, for top-hat photometric redshift bins centred at $z = 0.5$ and $z = 1.065$. For clarity, we only present errors for the models with RSD. Data are plotted for two redshift bins, and we clearly see that the increase in volume surveyed at high redshifts leads to more precise clustering measurements.

3 TESTING WITH MOCKS

This section outlines tests of our analytic prediction for the model $w(\theta)$ and its covariance matrices, performed using mock catalogs drawn from the N-body simulation MICE7680 produced by the MICE collaboration. This simulation assumed a flat ΛCDM cosmology with parameters $\Omega_m = 0.25, \Omega_b = 0.044, \sigma_{8,\rm mass}(0) = 0.8, n_s = 0.95$ and $h = 0.7$ and tracked the gravitational evolution of 2048^3 dark-matter particles within a comoving volume with a box size given by $L_{\rm box} = 7680\,h^{-1}\,$Mpc (see Fosalba et al. 2008 and Crocce et al. 2010a for further details). We use mock catalogues corresponding to dark matter particles distributed in slices of varying width centered at the mean redshift of z=0.5 (i.e. extracted from the co-moving output at this z) and subtending 1/8 of the sky. The very large volume of MICE7680 allow us to obtain at least 125 independent mocks for every bin-width and photometric error under consideration[2]. We refer the reader to C10 for a detailed presentation of the mock build-up.

3.1 Pair-centre Covariance

We use the mocks to test our estimation of the pair-centre covariance matrix. We note that the theoretical modelling of w_{TH} and its covariance matrix has been extensively tested against the mocks in C10. Using a range in redshift $0.2 < z < 0.8$, the volume was split, in photometric-redshift-space, into shells $15h^{-1}$Mpc thick. We then calculated $w_{pc}(\theta)$ for each realization by measuring all of the correlation- and cross-correlation functions of shells where $0.475 < (z_i + z_j)/2 < 0.525$, where z_i is the mean redshift of slice i, and then summing them according to the overall redshift distribution. These measurements allow us to calculate the covariance matrix for $w_{pc}(\theta)$ for the pair-centre bin $0.475 < z_{pc} < 0.525$. Fig. 3 presents the diagonal elements of the covariance matrix, multiplied by 10^8, determined from the mocks (red squares) and from Eq. 22 using shells 0.01 thick in photometric-redshift-space (black triangles). The theory appears to slightly underestimate the variance on large scales and slightly over-estimate the variance on small scales. However, the agreement is close enough that we should be able to use Eq. 22 for the purposes of this study. We find that the agreement between off-diagonal terms is quite similar, in terms of the absolute differences between the theoretical and mock estimates.

3.2 Constraining $f(z)\sigma_8(z)$

While the model w_{TH} and its covariance matrix has already been shown to agree with the mocks (see C10), we wish to confirm

[2] Mock catalogs are publicly available at http://www.ice.cat/mice

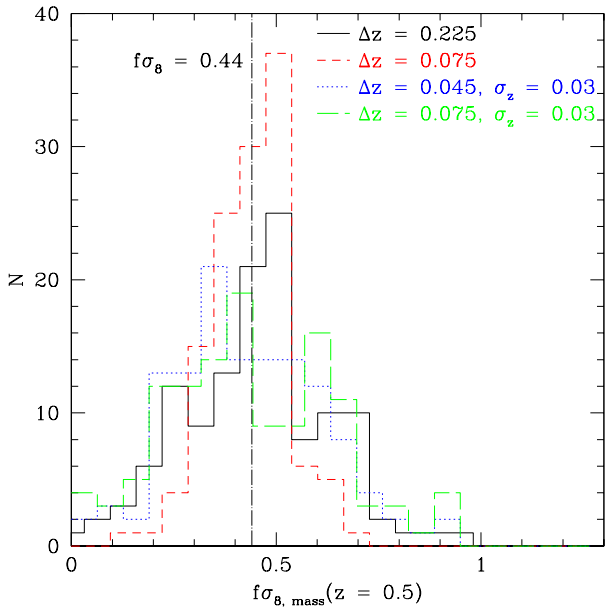

Figure 4. Histograms displaying the distribution of $f(z)\sigma_8(z)$ values obtained from 125 MICE mock catalogs with $\bar{z} = 0.5$ and $\Delta z = 0.15(1+z)$ (solid black line) and $\Delta z = 0.05(1+z)$ (dashed red line) with no redshift error, for a mock catalog with $\Delta z = 0.03(1+z)$ and redshift errors $0.02(1+z)$ (dotted blue line), and for a mock catalog with $\Delta z = 0.05(1+z)$ and redshift errors $0.02(1+z)$ (long-dashed green line).

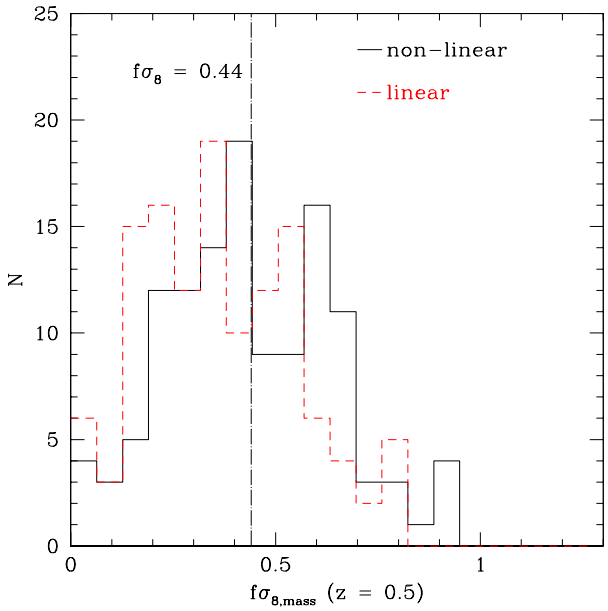

Figure 5. Histograms displaying the distribution of $f(z)\sigma_8(z)$ values obtained from MICE mock catalogs with $\bar{z} = 0.5$, $\Delta z = 0.05(1+z)$, and $\sigma_z = 0.02(1+z)$, when non-linear effects are included in the modelling (solid black) and are not included in the modelling (dashed red).

that we can recover an unbiased value of $f(z)\sigma_8(z)$ and its uncertainty. We have tested four mock samples against the analytic predictions: two that assume no photometric redshift errors, with widths of $\Delta z = 0.05(1+z)$ and $\Delta z = 0.15(1+z)$ and two that have redshift errors $0.02(1+z)$ and $\Delta z = 0.03(1+z)$ and $\Delta z = 0.05(1+z)$ (all have RSD effects applied). We only test the predictions at medium redshift ($z \sim 0.5$), where we can select 125 non-overlapping samples from the MICE simulations. While we are testing the results at $z = 0.5$, we expect the DES to obtain much more precise constraints at higher redshifts. However, given that the distribution of matter becomes more non-Gaussian as the Universe evolves, we can reasonably expect that the modelling that works at $z \sim 0.5$ should work at higher redshift as well. Thus, by confirming that our modelling is correct at $z \sim 0.5$, we expect our modelling to be correct in general.

The mocks provide measurements of $w(\theta)$ with $0.2^o \leqslant \theta \leqslant 8^o$ in angular bins of width 0.2^o. Jack-knife errors, $\sigma_{jk}(\theta)$, (see, e.g., Scranton et al. 2002; Myers et al. 2007; Ross et al. 2007) are calculated for each of these 125 mocks, using 63 independent regions of equal area. In order to estimate the covariance matrix of each realization, we determine the covariance matrix of the ensemble of mocks, Cov_e, and use the covariance matrix, Cov_{jk} given by $\mathrm{Cov}_{jk}(\theta,\theta') = \mathrm{Cov}_e(\theta,\theta')\sigma_{jk}(\theta)\sigma_{jk}((\theta')/\sqrt{\mathrm{Cov}_e(\theta,\theta)\mathrm{Cov}_e(\theta',\theta')}$. We find that, in the case of the most extreme fluctuations from the mean, the size of the jack-knife errors of individual angular bins are correlated with the size of the fluctuation. Modulating the covariance matrix based on the jack-knife errors thus reduces the weight of the more extreme fluctuations and we find this yields results matching our analytic predictions.

To find the best-fit values of $f(z)\sigma_8(z)$, we fit for data in the range $1^o \leqslant \theta \leqslant 5^o$, **marginalizing over** $b(z)\sigma_8(z)$. In order to produce the models we compare to these mocks, we use the same power-spectrum used by the MICE collaboration (available at the MICE website). Fig. 4 presents histograms of these best-fit $f(z)\sigma_8(z)$ values obtained for four types of mock; $\Delta z = 0.15(1+z)$ in solid black, $\Delta z = 0.05(1+z)$ in dashed red, $\Delta z = 0.03(1+z)$ & $\sigma_z = 0.02(1+z)$ in dotted blue, and $\Delta z = 0.05(1+z)$ & $\sigma_z = 0.02(1+z)$ in long dashed green. For the mean and standard deviation of the two distributions without redshift errors, we find 0.47 ± 0.09 for $\Delta z = 0.05(1+z)$ and $0.48,\pm0.15$ for $\Delta z = 0.15(1+z)$. For $\sigma_z = 0.02(1+z)$, we find 0.42 ± 0.18 for $\Delta z = 0.03(1+z)$ and 0.43 ± 0.2 for $\Delta_z = 0.05(1+z)$.

We make analytic predictions, based on the modelling described in Section 2, using methods described fully in Section 4. These predictions are $f(0.5)\sigma_8(0.5) = 0.44 \pm 0.09$, $f(0.5)\sigma_8(0.5) = 0.44^{+0.13}_{-0.16}$, $f(0.5)\sigma_8(0.5) = 0.44^{+0.16}_{-0.18}$, and $f(0.5)\sigma_8(0.5) = 0.44^{+0.18}_{-0.20}$, respectively, for the four redshift bins described above. These agree quite well with the results from the mocks and therefore suggest that our analytic formalism can be used to effectively predict the precision to which $f(z)\sigma_8(z)$ can be measured with a DES-like survey. We further note that we have applied a linear RSD model (given by Eqs. 2-7) to obtain all of these results, and this does not appear to bias the results.

3.3 Importance of Non-linear Gravitational effects

The MICE simulations obviously include non-linear effects from the gravitational clustering in the distribution of matter, and we need to model these effects in order to match the recovered angular correlation function. If we do not add non-linear effects to the spatial correlation function (i.e., $\xi(r,z) = D^2(z)\xi_{lin}(r,0)$) when fitting to the data, we obtain a significantly different distribution of best-fit $f(z)\sigma_8(z)$ values. We note that in both cases we are still

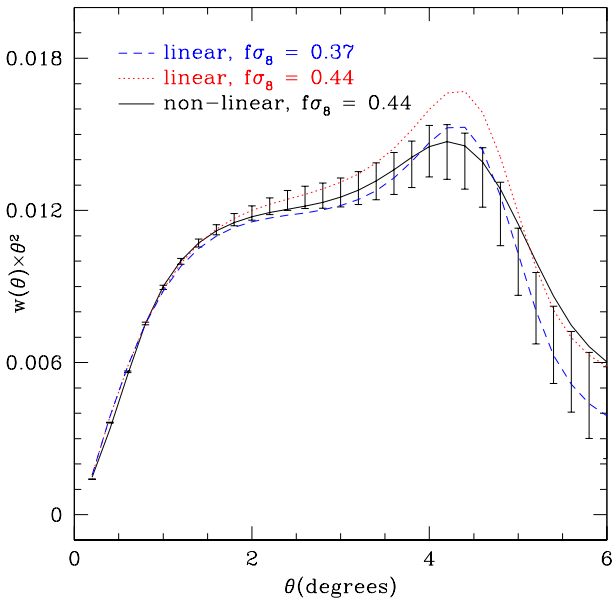

Figure 6. The mean angular correlation function from the MICE mocks for a redshift bin centred on $z = 0.5$, $\Delta z = 0.05(1+z)$, and $\sigma_z = 0.02(1+z)$ is shown by the black error-bars. The solid black curve displays the model $w(\theta)$ including non-linear effects and the LCDM prediction of $f(0.5)\sigma_8(0.5) = 0.44$. The dotted red curve displays the model when non-linear effects are not included and $f(0.5)\sigma_8(0.5) = 0.44$ and the dashed blue curve displays the model when non-linear effects are not included and $f(0.5)\sigma_8(0.5) = 0.37$ (that is the best-fit when non-linear effects are not included).

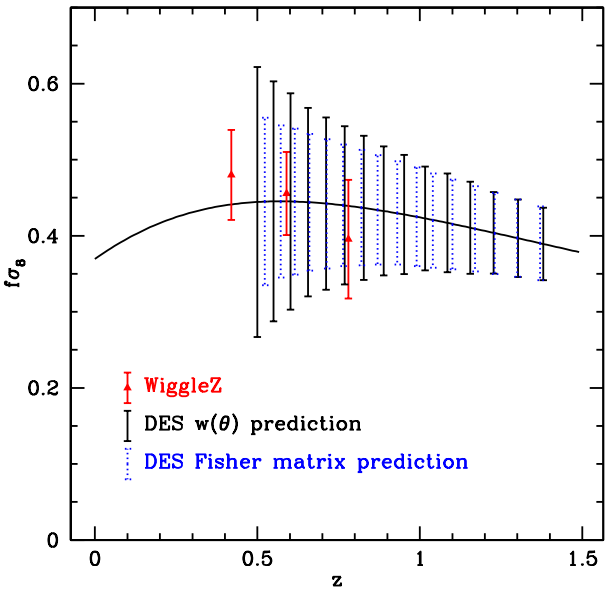

Figure 7. The solid line displays the model $f(z)\sigma_8(z)$ for our default ΛCDM model. 1σ errors (black) were calculated for the expected measurements made via successive top-hat photometric redshift bins for DES galaxies between $0.475 < z < 1.42$ and the blue error-bars display Fisher matrix predictions for similar redshift bins. The red points with 1σ errors are the measurements made with the WiggleZ survey (Blake et al. 2010).

using the linear model described by Eqs. 2-7 to apply the effects of RSD. The histogram of this distribution for the redshift bin with $\Delta z = 0.05(1+z)$ and $\sigma_z = 0.02(1+z)$ is displayed displayed in red in Fig. 5 (with the original histogram including non-linear effects displayed in black). The distribution is significantly skewed towards low $f(z)\sigma_8(z)$ values. The mean of the distribution decreases to 0.37 (from 0.43) — a 14 per cent change.

Fig. 6 shows model $w(\theta)\times\theta^2$ (curves) and the mean $w(\theta)\times\theta^2$ from the MICE mocks (black error-bars) for a redshift bin centred at $z = 0.5$, $\Delta z(1+z) = 0.05$, and $\sigma_z = 0.02$. The black curve displays the model including non-linear effects and $f(0.5)\sigma_8(0.5) = 0.44$ (that is the standard ΛCDM prediction at $z = 0.5$). The red curve displays the model without non-linear effects and $f(0.5)\sigma_8(0.5) = 0.44$, and the blue-curve displays the same model for $f(0.5)\sigma_8(0.5) = 0.37$ (that is the best-fit when the non-linear effects are not included). Essentially, the non-linear effects soften the BAO peak, and when they are not included in the models, the data is best-fit by a model with a smaller $f(z)\sigma_8(z)$ in order to compensate. We note that the error-bars displayed are not the standard deviations, σ_M, of the mocks but the errors in their mean (i.e., $\frac{1}{\sqrt{N}}\sigma_M$ and there are $N = 125$ mock realizations). Thus, the disagreement at large scales between the model (black curve) and the mocks is at the $\sim 1\sigma$ level. Given that the $f(z)\sigma_8(z)$ values determined from the mocks agree with the analytic predictions, this disagreement at large scales is too slight to significantly bias our results.

We find that the best-fit value of $f(0.5)\sigma_8(0.5)$ has shifted by 14 per cent when we do not include non-linear effects. The main non-linear contribution is due to the damping of the BAO due to large-scale velocity flows. This effect thus grows as the Universe evolves (see, e.g., Appendix A of C10). This implies that we expect the linear theory to yield a less biased result at higher redshift. This is indeed the case. We can use our theoretical predictions to find the linear model $w(\theta)$ that is the best-fit to the non-linear model $w(\theta)$. At $z = 0.7$, we find decreasing the value of $f(0.7)\sigma_8(0.7)$ by 8 per cent best matches the non-linear model, and that at $z = 1.0$, decreasing the value of $f(1.0)\sigma_8(1.0)$ by 6 per cent yields the best-fit to the non-linear model. While the magnitude of the bias does decrease with redshift, it is quite clear that accurate non-linear modelling of $w(\theta)$ is required to obtain accurate values of $f(z)\sigma_8(z)$.

4 MEASURING REDSHIFT-SPACE DISTORTIONS IN THE DES

Fig. 2 shows that RSD will significantly affect the angular clustering measured from DES for top-hat bins. We now quantify the constraints that could be possible for the DES. The blue error-bars in Fig. 7 represent the uncertainty that one obtains from Fisher matrix predictions for the full-anisotropic 3D power spectrum for the DES. These were calculated using the method described in White et al. (2009), with a radial damping term for the power spectrum of the form $e^{-(k\sigma_z\mu)^2}$, where we assume the photometric redshift error σ_z is the dominant cause of radial damping (and μ remains the cosine of the angle to the line of sight). These predictions are for successive bins of width 0.03(1+z), the minimum redshift of the first bin being 0.5, and $\sigma_z = 0.03(1+z)$.

We now consider how closely we can match the Fisher matrix errors using angular clustering measurements. We shall use the angular correlation function for pair centre binning, w_{pc}, which is

independent of RSD, to measure $b(z)\sigma_8(z)$. The angular correlation function for top-hat binning depends on both $f(z)\sigma_8(z)$ and $b(z)\sigma_8(z)$, so the combination of the two measures both. Thus, despite the relative weakness of the signal-to-noise of w_{pc} (see Fig. 1), the fact that w_{pc} is independent of $f(z)\sigma_8(z)$ allows us to break the $f(z)\sigma_8(z)$ - $b(z)\sigma_8(z)$ degeneracy inherent in most clustering measures. (Though, it should be noted that the Fisher matrix prediction does not include the information about pairs outside of the photometric redshift slice.)

We assume that all binned correlation function measurements are drawn from a multi-variate Gaussian distribution, with covariance matrices calculated as described in Section 2.1. Thus, we calculate the standard χ^2 statistic, constructing the full covariance matrix from those of w_{TH} (Eq. 13) and w_{pc} (Eq. 22) and estimating $\mathrm{Cov}_{TH,pc}$ as described at the end of section 2.2. We are therefore able to find the range of $f(z)\sigma_8(z)$ values that take up 68 per cent of the likelihood space around the Likelihood Maximum, while marginalising over the uncertainty to which the bias can be measured.

We constrain the range of angles used in these constraints to be such that $20h^{-1}$ Mpc$< r_{eq} < 100h^{-1}$ Mpc, where $r_{eq} = 2x(\bar{z})\tan(\theta/2)$ (with θ in radians) and $x(z)$ is the co-moving distance to the median redshift, $\bar{z}$, of sample of galaxies we consider (this has been shown by, e.g., C10 to be an appropriately small scale to which the modelling is still accurate). We use 15 contiguous top-hat photometric redshift bins, and 15 matched pair-centre bins between $0.475 < z < 1.42$, each of width $0.0333(1+z)$, so the first bin has $0.475 < z < 0.525$ and the last $1.34 < z < 1.42$. (The fact that Fig. 1 of C10 suggests the mean photometric redshift uncertainties are expected to $\sim$ constant over the range $0.45 < z < 1.4$ justifies our chosen redshift range.) We conservatively assume that we can select 7 million galaxies in each redshift bin, with good photometric redshifts ($\sigma_z \sim 0.03(1+z)$) out of a total of 300 million galaxies: the approximate DES galaxy density distribution shows that we should expect more than 10 million galaxies in each bin in total.

The expected constraints from these angular clustering measurements are shown in Fig. 7, compared with the Fisher matrix predictions. At high redshift, the predictions are nearly identical, but at low redshift the Fisher matrix predicts better constraints than using the angular clustering method described above. This is considered further in the next section, where we determine that the optimal bin at $z \sim 1$ is $\sim 0.03(1+z)$, but at $z \sim 0.5$, a narrower bin recovers better constraints. We have also plotted recent measurements made using the WiggleZ survey (Blake et al. 2010) in Fig. 7. WiggleZ already does better than DES at its redshifts, but beyond the redshift limits of WiggleZ ($z \sim 0.8$), DES will provide competitive measurements with better than $\sim$20% error for slices of width $\Delta z = 0.03(1+z)$. We note that the $f(z)\sigma_8(z)$ constraints between separate redshift bins are highly correlated with each other. We take these correlations into account when determining how well the DES constrains $f(z)\sigma_8(z)$ over its full redshift range in section 4.2.

4.1 Optimizing the Method

The size of the effect of RSD on angular clustering measurements is strongly dependent on the characteristics of the sample, and in particular the true radial size of the redshift slice is one of the most important factors. This is given by a convolution between the photometric redshift bounds of the bin and the photometric redshift distributions. The mean bias of the galaxies is also important, as

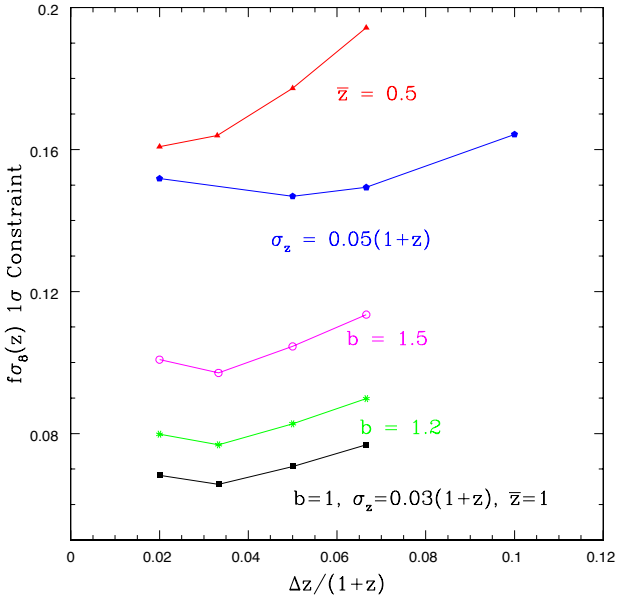

Figure 8. The black points show the expected error on $f(z)\sigma_8(z)$ versus the width of the photometric redshift bin, for unbiased tracers with average photometric redshift error $\sigma_z = 0.03(1+z)$, selected from redshift bins centred on $z = 1.065$. The other lines display the same information, for samples changed as labeled.

the relative amplitude (compared to the real-space clustering) of the redshift distortion effect is inversely proportional to the bias.

Fig. 8 displays the expected error on $f(z)\sigma_8(z)$, for various possible data samples. The black line is for unbiased tracers centred at $z = 1.065$ and with $\sigma_z = 0.03(1+z)$, which gives a minimum in the expected error for the bin $\Delta z(1+z) = 0.033(1+z)$. This represents a balance between the number of galaxies in each sample against the size of the RSD signal. The blue line shows the effect of a sample selected with larger photometric redshift errors, now $0.05(1+z)$. The expected error on $f(z)\sigma_8(z)$ is more than twice as high, and the minimum is at a larger bin width. The true bin width is determined by a convolution between the photometric redshift bounds of the bin and the photometric redshift distributions so decreasing the photometric redshift limits has less of an effect when σ_z is increased.

Fig. 8 also shows that the effect of increasing b has a detrimental effect on the RSD measurements: a 50 per cent increase in the average galaxy bias results in a $\sim$ 50 per cent increase in the predicted RSD error. (The error on $\beta = f/b$ remains constant, implying the error $f(z)\sigma_8(z)$ is proportional to the bias.) This is an important consideration for the selection of galaxy samples, particularly at high redshifts where the samples have larger biases (see, e.g., Zheng et al. 2007), as do red galaxies that currently have the lowest photometric redshift errors.

At lower redshifts, Fig. 8 shows that RSD measurements are strongly degraded by the significantly smaller volume available. At these redshifts, the error decreases significantly with bin size, down to the most narrow bin we test, $\Delta z(1+z) = 0.02(1+z)$, though it does appear to asymptote to ~ 0.16. This is due to the fact that the number densities are so high at this redshift that decreasing the total number of galaxies has a minimal effect on the error on $w(\theta)$. It is clear from Fig. 8 that the choosing the optimal sample with which to measure RSD depends on a complicated balance of many

interdependent factors: this can only reliably be achieved after all of the data is in hand.

4.2 Cosmological Constraints from full Redshift Range

We now consider cosmological constraints from the combination of measurements at different redshifts. We account for the covariance in $f(z)\sigma_8(z)$ between redshift bins by assuming that their Pearson coefficient is equal to the Pearson coefficient that defines the covariance of $w(\theta)$ between different redshift bins. We determine the covariance of $w(\theta)$ between different redshift bins by assuming (see, e.g., Thomas et al. 2010)

$$\mathrm{Cov}(C_\ell^i, C_\ell^j) = \frac{1}{(2\ell+1)}(C_\ell^{i,j})^2 \quad (25)$$

and then substituting $\mathrm{Cov}(C_\ell^i, C_\ell^j)$ for $\sigma^2(C_\ell^{i,j})$ in Eq. 13, yielding $\mathrm{Cov}(w(\theta_1)^i, w(\theta_2)^j)$. We find that the Pearson coefficient given by $\mathrm{Cov}(w(\theta_1)^i, w(\theta_2)^j)/\sqrt{\mathrm{Cov}_{i,i,\theta_1,\theta_2}\mathrm{Cov}_{j,j,\theta_1,\theta_2}}$ is nearly independent of θ_1, θ_2. Thus, we set

$$\mathrm{Cov}_{f,i,j}/\sqrt{\mathrm{Cov}_{f,i,i}\mathrm{Cov}_{f,j,j}} = \mathrm{Cov}(w^i, w^j)/\sqrt{\mathrm{Cov}_{i,i}\mathrm{Cov}_{j,j}} \quad (26)$$

where $\mathrm{Cov}_{f,i,j}$ is the covariance in $f(z)\sigma_8(z)$ between redshift bins i and j. We find that if we make Gaussian realizations of our simulated data matching the covariance matrix for correlation functions expected for two adjacent redshift bins, the covariance between measurements of $f(z)\sigma_8(z)$ recovered is within 10% of what we estimate using Eq. 26 (and is not systematically offset). Thus, we use Eq. 26 to construct our full covariance matrix for $f(z)\sigma_8(z)$, given its relative ease in computation and that it should be sufficiently accurate for our tests.

4.2.1 *Constant offset for $f(z)\sigma_8(z)$*

If we consider deviations around our fiducial model with a redshift-independent offset in $f(z)\sigma_8(z)$, then the 68% confidence interval for $\Delta f(z)\sigma_8(z)$ is given by

$$\Delta\left(f(z)\sigma_8(z)\right) = 1/\sqrt{\sum_{i,j}\mathrm{Cov}^{-1}_{f,i,j}}. \quad (27)$$

We determine $\Delta\left(f(z)\sigma_8(z)\right)$ for unbiased tracers occupying a variety of bin widths (all with the median redshift of the first bin at 0.5 and the median redshift of the final bin less than 1.4; the number of galaxies in each bin is assumed to be $7\times10^6 \times (\Delta z(1+z)/0.05)$) and plot the results in Fig. 9. We find that, for $\sigma_z = 0.03(1+z)$, $\Delta\left(f(z)\sigma_8(z)\right)$ asymptotes towards a value of 0.025. For $\sigma_z = 0.05(1+z)$ the decrease in the error as a function of bin width is much stronger, but at the minimum bin width we probe ($0.02(1+z)$) we find $\Delta\left(f(z)\sigma_8(z)\right) = 0.06$ — more than twice as large as for $\sigma_z = 0.03(1+z)$.

We also investigate a scenario with more realistic evolution in the bias of the galaxies selected, assuming $b(z) = 0.5 + z$. This allows the bias to be unity at $z = 0.5$ and gives a similar value to the bias of galaxies in the DEEP2 field (see, e.g., Zheng et al. 2007) at $z = 1$. For this bias model, we find $\Delta\left(f(z)\sigma_8(z)\right)$ asymptotes towards 0.04. Overall, this suggests that DES alone should be able to rule out models that cause the growth history to differ by more than 10 per cent from the ΛCDM prediction. It further suggests that, though the covariance between bins grows large (the reduced covariance of off-diagonal terms is as large as 0.9), extra information can be gained by making the bins as narrow as possible.

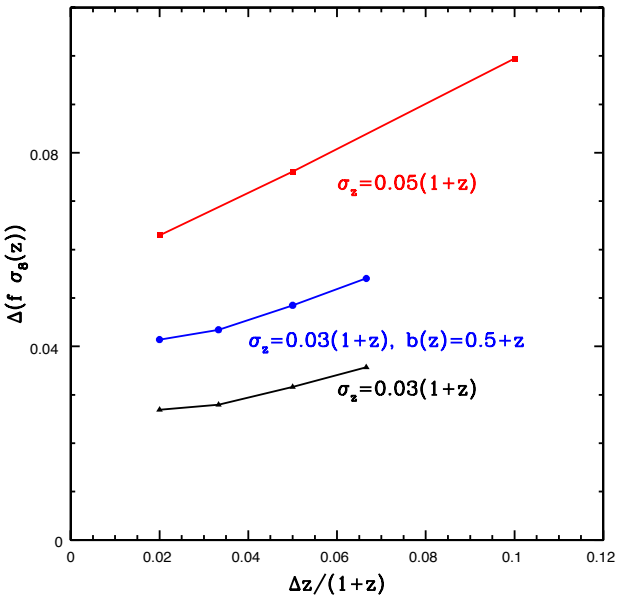

Figure 9. 68% confidence limits for a constant offset in $f(z)\sigma_8(z)$ from our fiducial model, when we combine the constraints produced by a series of $w_i(\theta)$ measured in successive redshift bins with median redshifts between 0.5 and 1.4, versus the width of the photometric redshift bins. The black symbols show the prediction for unbiased tracers with average photometric redshift error $\sigma_z = 0.03(1+z)$. The red points display the same information for $\sigma_z = 0.05(1+z)$ and the blue points assume that the bias of the selectable galaxies evolves, such that $b(z) = 0.5+z$ and the average photometric redshift error of these galaxies is $\sigma_z = 0.03(1+z)$.

4.2.2 *Deviations in γ*

One can also determine how well DES will be able to constrain models of the type $f(z) = \Omega_m(z)^\gamma$ (see, e.g., Linder 2005). We note that this also implies a change in the behaviour of $\sigma_8(z)$, since $\sigma_8(z) = \sigma_8(0)G(z)$ and $f(z) = \mathrm{dlog}(G)/\mathrm{dlog}(a)$. We fix the value of $\sigma_8(1088)$ that yields $\sigma_8(0) = 0.8$ in the ΛCDM cosmology and determine the expected behaviour of $f(z)\sigma_8(z)$. We then test this against the $f(z)\sigma_8(z)$ covariance matrix we obtain for a series of $w_i(\theta)$ measurements to predict the ability of DES to constrain γ. The results we find are presented in Fig. 10. We find there is a steady decrease in the expected error on γ as the bin width deceases, and we find that DES alone should be able to place 1σ constraints on the value of γ to less than 0.25, even with realistic evolution in the bias of the observed galaxies.

5 ROBUSTNESS TO UNDERLYING COSMOLOGY AND PHOTOMETRIC REDSHIFT SYSTEMATICS

The RSD constraints presented in the previous section assumed perfect knowledge of cosmological geometry and photometric redshift errors. Both changing the assumed cosmology and introducing systematic errors can cause scale dependent effects that could mimic the effects of redshift-space distortions when measuring $w(\theta)$ using a top-hat bin.

Measurements of the angular correlation function only depend on angles and redshifts, and are therefore independent of cosmological model: a model does not have to be specified in order to make these measurements. The cosmological dependence

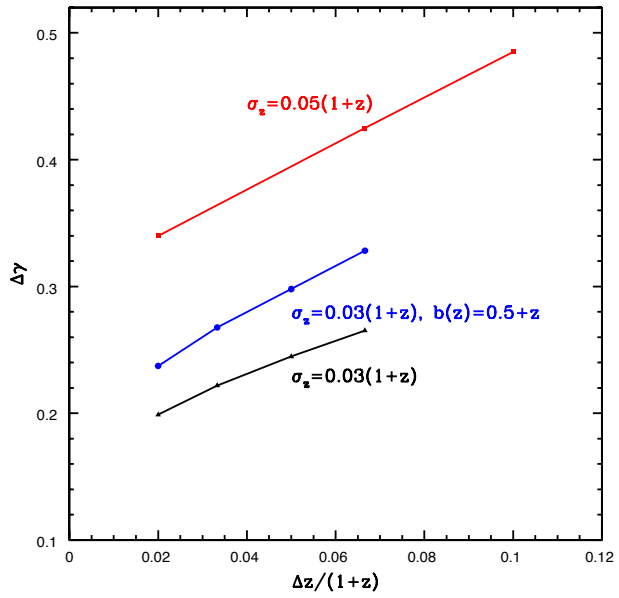

Figure 10. As Fig. 9, but now showing the expected constraints on the value of γ, given the model $f(z) = \Omega_m(z)^\gamma$.

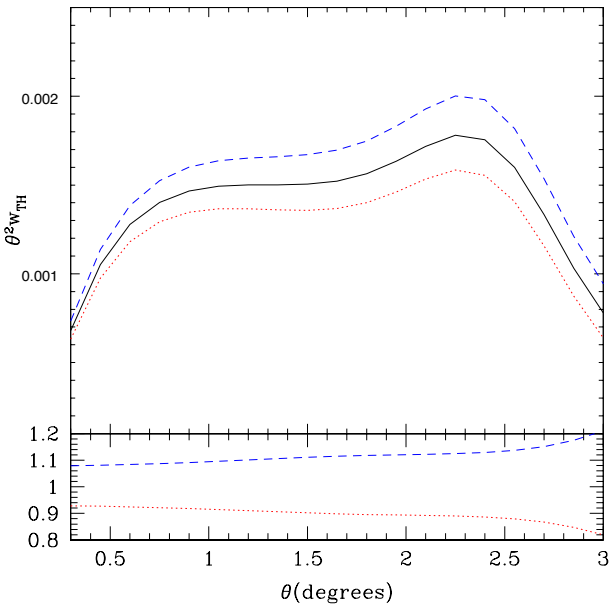

Figure 11. The top panel displays the model $w(\theta)$, multiplied by θ^2 from the top-hat bin defined by $1.0 < z < 1.13$ with $\sigma_z = 0.03(1+z)$ (black line), $\sigma_z = 0.033(1+z)$ (red dotted line) and $\sigma_z = 0.027(1+z)$ (blue dashed line). The bottom panel displays the ratio of the models with $\sigma_z = 0.033(1+z)$ and $\sigma_z = 0.027(1+z)$ to the model with $\sigma_z = 0.03(1+z)$.

only arises through the model to be fitted to the data. We test the systematic effect of assuming an incorrect background model on $f(z)\sigma_8(z)$ measurements by using the $1 < z_{phot} < 1.13$ redshift bin. In effect, we consider fitting to a fixed ΛCDM model with free structure growth, and determine the degree to which the inferred structure growth changes when the assumed ΛCDM parameters are incorrect.

We calculate the value of $f(z)\sigma_8(z)$ one measures if one assumes the geometrical cosmology given by $\Omega_m = 0.25, f_b = \Omega_b/\Omega_m = 0.18, h = 0.7$, but the Universe has a true cosmology that is different. For $(f_b)_{true} = 0.2$, the best-fit value of $f(z)\sigma_8(z)$ increases to 0.52 ± 0.07 (from the true value of 0.42 ± 0.07) while it decreases to $f(z)\sigma_8(z) = 0.31^{+0.09}_{-0.08}$ for $(f_b)_{true} = 0.16$. Changing Ω_m produces an even more significant effect, as the $f(z)\sigma_8(z)$ decreases to $0.23^{+0.09}_{-0.10}$ when $(\Omega_m)_{true} = 0.3$. While these changes to the cosmology are within the 95% confidence limits determined by WMAP (Komatsu et al. 2009), by the time that DES finishes, the Planck Experiment will have set tighter constraints on these parameters, making this effect less important. However, given current constraints, a joint fit to all of the parameters is clearly required.

There are other effects that can cause scale dependent changes to the observed $w(\theta)$. Any scale dependent bias will clearly be a problem, and it has recently been shown that large halos display scale dependent biases (see, e.g., Smith et al. 2008; Manera & Gaztañaga 2009; Desjacques et al. 2010). However, as shown in Fig. 8, the best RSD constraints will be obtained from objects that reside in the least biased halos, for which we expect the least scale-dependent bias. Any non-zero f_{NL} will also cause a scale dependent bias, though for $|f_{NL}| \sim 100$, this is a much smaller effect than RSD at scales smaller than the BAO scale. Additionally, we may worry about observational systematics, such as Galactic extinction or stellar contamination. Ross et al. (2011) has shown that a thorough accounting of and correction for such systematics and their effects is possible, but depending on the particular survey, this could translate to additional systematic errors in estimation of $f(z)\sigma_8(z)$. We note that the systematic effects are largest at scales greater than the BAO scale, and are therefore less likely to strongly affect measurements of $f(z)\sigma_8(z)$.

5.1 Incorrect Redshift Distributions

One might worry that the determination of $f(z)\sigma_8(z)$ (or any other cosmological parameter) will be particularly sensitive to misestimation of the true redshift distribution of galaxies within a particular redshift bin. In order to investigate this, we alter the σ_z and also simulate the effect of a redshift dependent bias in our modelling. Previously, we assumed $\sigma_z = 0.03(1+z)$ for the DES galaxies, and we now contrast against models calculated increasing or decreasing this assumed error by 10%. This is about the same as the average uncertainty in σ_z stated in the DES requirements document, which states that the uncertainty in the dispersion in any photometric redshift bin of width $0.1(1+z)$ should be less than 0.003.

The effect on the top-hat measurement of changing σ_z is shown if Fig. 11. Its amplitude changes by ~ 10 per cent, but its shape remains very similar. The bottom panel of Fig. 11, shows that there is a slight scale-dependency in the change in amplitude, similar to what C10 find (as displayed in their Fig. 6). Figs. 12 and 13 display the same information as Fig. 11 for the pair-centre measurement and the ratio of the top-hat measurement to the pair centre measurement, respectively. The pair-centre measurement displays almost no dependence on σ_z. The pair-centre measurements change by less than 2%, and the change in the top-hat bin is closer to 10%. Further, at small scales, where the redshift distortion effect is relatively small, the ratio between the different pair-centre measurements differs by < 0.5 %. This implies that the pair-centre measurement would continue to allow for an accurate measure of $b(z)\sigma_8(z)$. However, this value of $b(z)\sigma_8(z)$ would cause the

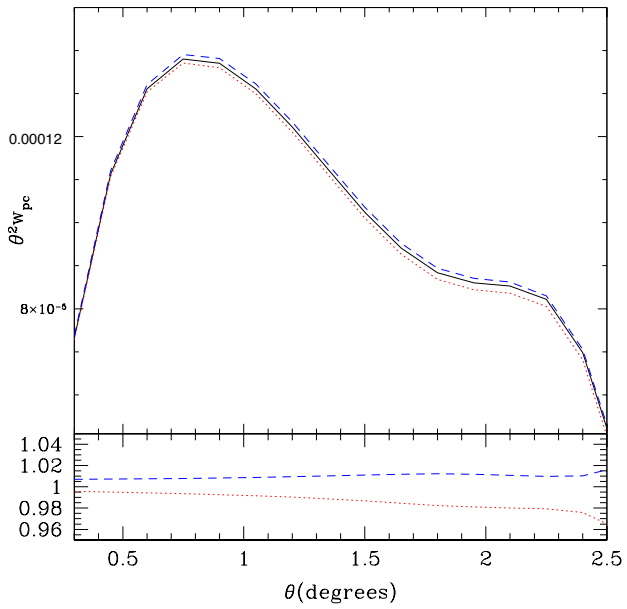

Figure 12. The model pair-centre measurements for the three situations described in Fig. 11.

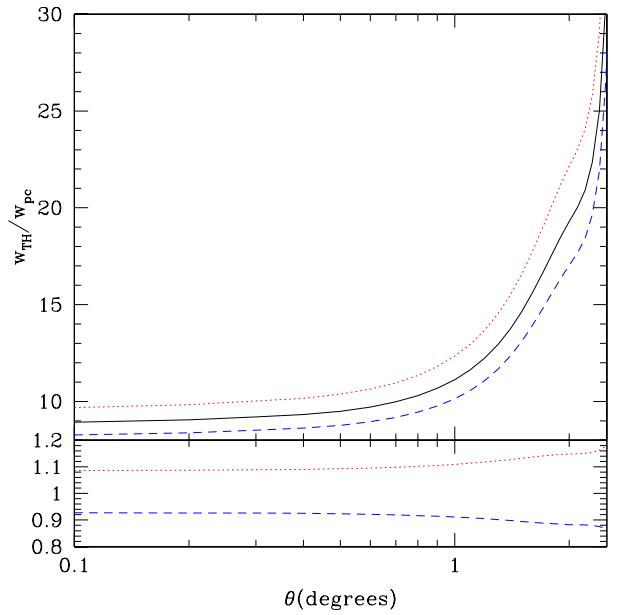

Figure 13. Same as Fig. 11, but the ratio between the model top-hat and model pair-centre measurements are plotted instead, and the θ axis is scaled logarithmically.

model top-hat $w(\theta)$ to differ by $\sim$ 10 per cent from the measured $w_{TH}(\theta)$ on scales $< 20h^{-1}$Mpc, regardless of the value of $f(z)\sigma_8(z)$ (since RSD do not have a significant effect on the amplitude at these scales).

The mismatch between the two measurements on small scales allows one to discover and fix errors in the estimation of the true redshift distribution, in a way that is relatively independent of RSD. Consider the ratio of the top-hat to pair-centre $w(\theta)$: For the ratio, the values of $b(z)\sigma_8(z)$ cancel each other (and one would expect any non-linear bias to cancel as well). This implies that even at small scales, where proper modelling of $w(\theta)$ of galaxies requires knowledge of the halo occupation distribution of the galaxies, the ratio would remain constant. (Note, at large scales, it is the linear effect of RSD that causes the ratio to be non-constant.) At small-scales, the top-hat and pair-centre measurements should probe the same real-space clustering, i.e., where $w(\theta)$ behaves as a power-law, we would expect the pair-centre and top hat measurements to have the same slope. Thus, we expect the ratio to be independent of any non-linear effects. This implies that, at small scales, any offset between the measured ratio and the theoretical ratio will be due almost entirely to incorrect modelling of the true redshift distributions.

At scales where $w(\theta)$ behaves as a power-law, the amplitude of $w(\theta)$ is proportional to

$$W(\sigma_z) = \int n^2(z,\sigma_z)H(z)dz. \quad (28)$$

Thus, one can determine how σ_z needs to be changed in order for $W(\sigma_{z,a})/W(\sigma_{z,m})$ (where $\sigma_{z,a}$ is the adopted mean photometric redshift error and $\sigma_{z,m}$ is the mean from the actual data) to match the offset found between the the measured and predicted ratios between the top-hat and pair centre measurements. When the errors are 10 per cent too small, the offset is 1.083, and we find that changing σ_z from 0.0027 to 0.0302 produces a matching $W(\sigma_{z,a})/W(\sigma_{z,m})$. When the errors are 10 percent too large, the offset is 0.922, and changing σ_z from 0.033 to 0.0298 produces a matching $W(\sigma_{z,a})/W(\sigma_{z,m})$. In both cases, a slight over-correction was required, but the correction would reduce the systematic error on any $f(z)\sigma_8(z)$ estimate to less than 1 percent.

In practice, one will have a individual photometric redshift errors (or PDFs) for each galaxy. In this case, the correction would be to find the (likely constant) factor by which each error distribution needs to widened or narrowed in order to achieve the desired ratio in the model. This correction is likely to be important for any analysis one wishes to conduct on the clustering of photometrically selected galaxies, and it is appealing because does not require any data external to the survey (unlike other proposed methods, which rely on smaller spectroscopic surveys, see, e.g. Newman 2008).

We also investigate the effect of a bias on the photometric redshifts (i.e., the mean photometric redshift in a bin may be higher or lower than the mean of the true redshift distribution). We apply a positive or negative photometric redshift bias of 0.01. This level of bias is close to 10 times higher than the $0.001(1+z)$ stated in the DES requirements document. The effect of these biases is seen in Fig. 14. The model top-hat $w(\theta)$ with no bias is shown by the black line, while red line is for $z_b = 0.01$, and blue $z_b = -0.01$. The value of the amplitudes changes only slightly — by $\sim$1 per cent. This is because the main effect is a change in the median redshift and thus the effective value of the linear growth rate. The ratio of $D(1.055)/D(1.075)$ is just 1.01, thus the results we find match the expectation. These results suggest that the requirements of DES will mean that photometric redshift bias is not an issue for the purposes of measuring $f(z)\sigma_8(z)$.

6 CONCLUSIONS

We have described the effects of RSD on angular clustering measurements and outlined an effective method for measuring $f(z)\sigma_8(z)$. In order to guide these efforts, we have extended the techniques outlined in C10 to model the amplitude and covariance

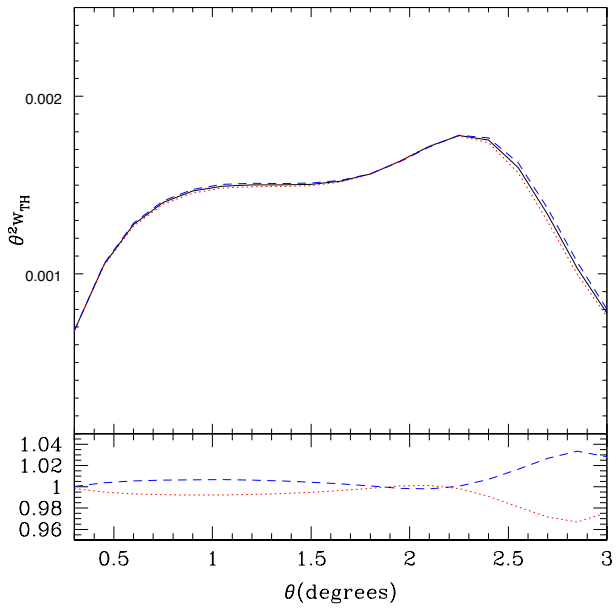

Figure 14. The top panel model $w(\theta)$ for a top-hat bin defined by $1.0 < z < 1.13$. The black line assumes no photometric redshift bias, while the red dotted line assumes a bias 0.01, and the blue dashed line assumes a bias of -0.01, all for $\sigma_z = 0.03(1+z)$. The bottom panel displays the ratio of the models with bias to the model with an unbiased distribution.

of $w(\theta)$ measured using galaxies selected from a DES-like survey, allowing us to determine the optimal binning scheme to extract the most information about RSD. In particular:

• We have shown that RSD have a measurable effect on the angular correlation function $w(\theta)$ measured using photometric redshifts. At the very least, any accurate model must include their effects, or have shown that they are negligible.

• We describe how using measurements $w(\theta)$ in pair-centre bins allows $b(z)\sigma_8(z)$ to be constrained independently of RSD, thereby minimizing the degeneracy between $b(z)\sigma_8(z)$ and $f(z)\sigma_8(z)$.

• We have shown that $f(z)\sigma_8(z)$ can be measured to $\sim 17 \times b$ per cent accuracy at $z = 1$ for a DES-like survey, assuming $\sigma_z = 0.03(1+z)$.

• We confirm that our analytic predictions of the ability to constrain $f(z)\sigma_8(z)$ work well as, when we measure $f(z)\sigma_8(z)$ from mock catalogs generated by the MICE simulation, we obtain distributions that agree with our analytic predictions.

• We show that omitting non-linear gravitational effects around the BAO scale in the modelling of $w(\theta)$ can cause the expected $f(z)\sigma_8(z)$ value one measures to be more than 15 per cent smaller than its true value.

• The accuracy with which $f(z)\sigma_8(z)$ can be measured depends strongly on the error on the photometric redshifts. At redshift 1, the expected error on $f(z)\sigma_8(z)$ is $\sim$ twice as large for $\sigma_z = 0.05(1+z)$ compared to $\sigma_z = 0.03(1+z)$. Given that the expected error depends strongly on the bias of the galaxies and the photometric redshift limits applied to the bin, we expect the optimal bin (or series of bins) can only be determined after the data is in hand.

• We have shown that, after adopting a reasonable expectation of $b(z)$, a series of $w(\theta)$ measurements made for galaxies drawn from narrow ($\Delta z(1+z) < 0.02$) redshift slices over the range $0.5 < z < 1.4$ should allow a DES-like survey to detect 10 per cent deviations from the ΛCDM prediction for cosmological growth of structure. In terms of the model $f(z) = \Omega_m(z)^\gamma$, we expect a DES-like survey to be able to determine $\gamma = 0.557^{+0.25}_{-0.22}$.

• We further show how the ratio can be used to correct any inaccuracy in the estimation of σ_z for a particular redshift distribution. This provides an attractive method for testing the photometric redshifts, since it does not require any external data.

The constraints that we predict will only improve as the redshift limits and sky area increase with future surveys. Given purely photometric data, it is clearly still worth investigating and measuring the effects of RSD.

ACKNOWLEDGEMENTS

We thank an anonymous referee for comments and suggestions that have improved the quality of this work.

We acknowledge the use of mock catalogues built upon an N-body simulation provided by the MICE collaboration (publicly available at http://www.ice.cat/mice). The MICE simulations have been developed at the MareNostrum supercomputer (BSC-CNS) thanks to grants AECT-2006-2-0011 through AECT-2010-1-0007. Data products have been stored at the Port d'Informaci Cientfica (PIC).

AJR and WJP thank the UK Science and Technology Facilities Council for financial support. WJP is also grateful for support from the Leverhulme trust and the European Research Council.

MC & EG acknowledge support from the Spanish Science Ministry: AYA2009-13936, Juan de la Cierva and Consolider-Ingenio CSD2007-00060, from Generalitat de Catalunya: project 2009SGR1398 and from the European Commissions Marie Curie Initial Training Network CosmoComp (PITN-GA-2009-238356).

REFERENCES

Alcock C., Paczynski B., 1979, Nat., 281, 358
Banerji M., Abdalla F. B., Lahav O., Lin H. (2008) MNRAS, 386, 1219
Ballinger W. E., Peacock J. E., Heavens A. F., 1996, MNRAS, 282, 877
Blake C., Collister A., Bridle S., Lahav O., 2007, MNRAS, 374, 1527
Blake, C., et al. 2010, MNRAS, 776
Cabre A., Gaztanaga E., 2009, MNRAS, 396, 1119
Colless M., et al., 2003, [[astro-ph/0306581]]
Cohn, J. D., 2009, [[arXiv:0503285v3]]
Crocce M., Fosalba P., Castander F. J., Gaztañaga E., 2010 MNRAS, 403, 1353
Crocce M., Cabre A., Gaztañaga E., 2010, [[arXiv:1004.4640]] C10
Desjacques, V., Crocce, M., Scoccimarro, R., Sheth, R. K., PRD, 82, 103529 (2010)
Dodelson, S. 2003, Modern cosmology / Scott Dodelson. Amsterdam (Netherlands): Academic Press. ISBN 0-12-219141-2, 2003, XIII + 440 p.,
Eisenstein D. J., Hu W. 1998, ApJ, 496, 605
Fisher K.B., Scharf C.A., Lahav O., 1993, MNRAS, 266, 219
Fosalba P., Gaztañaga E., Castander F. J., Manera M., 2010, MNRAS, 391, 435
Guzzo, L., 2009, Nature, 541, 2008
Hamilton A.J.S., 1992, ApJ, 385, L5

Hamilton A.J.S., "Linear redshift distortions: A review", in "The Evolving Universe", ed. D. Hamilton, pp. 185-275 (Kluwer Academic, 1998) [[astro-ph/9708102]]
Hawkins E. et al., 2003, MNRAS, 346, 78
Jackson, J. P. 1972, Ph.D. Thesis,
Kaiser N., 1987, MNRAS, 227, 1
Komatsu E. et al., 2009, ApJS, 180, 330
Linder E.V., 2005, PRD 72, 043529
Manera, M., Gaztañaga, E., e-print arXiv:astro-ph/0912.0446 (2009)
Myers, A. D., et al., 2007, ApJ, 658, 85
Newman, J. A. 2008, ApJ, 684, 88
Nock, K., Percival, W. J., & Ross, A. J. 2010, MNRAS, 407, 520 N10
Okumura T., Matsubara T., Eisenstein D.J., Kayo I., Hikage C., Szalay A.S., Schneider D.P., 2008, ApJ, 676, 889
Padmanabhan N., et al., 2007, MNRAS, 378, 852
Peacock J.A., et al., 2001, Nature, 410, 169
Percival W.J., et al., 2004, MNRAS, 353, 1201
Phillipps S., Fong R., Fall R. S. E. S. M., MacGillivray H. T., 1978, MNRAS, 182, 673
The *Planck* Collaboration, 2006, The Scientific Programme of *Planck*, [[astro-ph/0604069]]
Pope A.C., et al., 2004, ApJ, 607, 655
Ross A. J., Brunner R. J., Myers A. D., 2007, ApJ, 665, 67
Ross, A. J., Brunner, R. J., & Myers, A. D. 2008, ApJ, 682, 737
Ross, A. J., Percival, W. J., & Brunner, R. J. 2010, MNRAS, 407, 420
Ross, A. J., Tojeiro, R., & Percival, W. J. 2010, arXiv:1010.1403
Ross, A. J., et al. in prep.
Samushia, L., et al. 2011, MNRAS, 410, 1993
Samushia, L., Percival, W. J., & Raccanelli, A. 2011, arXiv:1102.1014
Sanchez E., et al., 2010, [[arXiv:1006.3226]]
Simpson F., Peacock J. A., 2010, Phys. Rev. D, 81, 043512
Smith, R., Scoccimarro & R., Sheth, R. K., PRD, 77, 043525 (2008)
Song Y.-S., Percival W. J., 2009, JCAP, 10, 4
Scranton R., et al., 2002, ApJ, 579, 48
Tegmark, M. 1997, Physical Review Letters, 79, 3806
Thomas, S. A., Abdalla, F. B., & Lahav, O. 2010, arXiv:1011.2448
White M., Song Y.-S., Percival W. J., 2009, MNRAS, 397, 1348
York D.G., et al., 2000, AJ, 120, 1579
Zehavi, I., et al., 2005, ApJ, 630, 1
Zheng Z., Coil A. L., Zehavi I., 2007, ApJ, 667, 760